Opening and tuning of band gap by the formation of diamond superlattices in twisted bilayer graphene

Andre R. Muniz[1] and Dimitrios Maroudas[2,*]

[1]*Departamento de Engenharia Química, Universidade Federal do Rio Grande do Sul, Porto Alegre, Brazil*

[2]*Department of Chemical Engineering, University of Massachusetts, Amherst, Massachusetts 01003, USA*

(Received 8 May 2012; revised manuscript received 6 July 2012; published 2 August 2012)

We report results of first-principles density functional theory calculations, which introduce a new class of carbon nanostructures formed due to creation of covalent interlayer C-C bonds in twisted bilayer graphene (TBG). This interlayer bonding becomes possible by hydrogenation of the graphene layers according to certain hydrogenation patterns. The resulting relaxed configurations consist of two-dimensional (2D) superlattices of diamondlike nanocrystals embedded within the graphene layers, with the same periodicity as that of the Moiré pattern corresponding to the rotational layer stacking in TBG. The 2D diamond nanodomains resemble the cubic or the hexagonal diamond phase. The detailed structure of these superlattice configurations is determined by parameters that include the twist angle, ranging from 0° to ∼15°, and the number of interlayer C-C bonds formed per unit cell of the superlattice. We demonstrate that formation of such interlayer-bonded finite domains causes the opening of a band gap in the electronic band structure of TBG, which depends on the density and spatial distribution of interlayer C-C bonds. We have predicted band gaps as wide as 1.2 eV and found that the band gap increases monotonically with increasing size of the embedded diamond nanodomain in the unit cell of the superlattice. Such nanostructure formation constitutes a promising approach for opening a precisely tunable band gap in bilayer graphene.

DOI: 10.1103/PhysRevB.86.075404 PACS number(s): 73.22.Pr, 73.22.−f, 61.46.Hk, 61.48.Gh

I. INTRODUCTION

Since its discovery in 2004,[1] graphene has attracted a tremendous amount of interest due to its unique physical properties that promise an extremely broad range of potential applications. Graphene is a zero-band-gap semiconductor (or semimetal), with valence and conduction bands touching at the Fermi level at the special K point in the first Brillouin zone (BZ); in the vicinity of this special point in reciprocal space, electrons have a linear energy-versus-momentum dispersion relation exhibiting the so-called Dirac cones and, as a result, they behave like relativistic particles as described by the Dirac equation.[2,3] An extremely important electronic property of graphene is its very high mobility of charge carriers, which enables electrons to travel submicrometer-long distances without scattering. Nevertheless, broad applications of graphene in microelectronics require the opening of a band gap in its electronic band structure. Toward this end, several approaches have been applied successfully, including chemical functionalization,[4–8] creation of graphene nanoribbons,[9] application of an electric field perpendicular to the graphene plane,[10] and insertion of defects, such as vacancies, for the creation of periodic antidot lattices.[11]

Chemical functionalization of single-layer graphene, such as hydrogenation and fluorination,[4–8] introduces sp^3-hybridized C-C bonds in the original graphene structure characterized by delocalized sp^2 C-C bonding of the C atoms in a honeycomb lattice arrangement. Such chemical functionalization alters the electronic and atomic structure of single-layer graphene. Typically, the introduction of such sp^3 bonds in graphene opens a band gap in its electronic band structure;[12,13] however, depending on the concentration and spatial arrangement of the chemisorbed atoms used for chemical functionalization, or more specifically, on the symmetry and the periodicity of the resulting superlattice of introduced defects, the Dirac cones at the K point may be preserved, with a reduction in the corresponding Fermi velocity.[14–16]

Control of the band gap by a generation of superlattices of defects in single-layer graphene (SLG) has been explored in depth in recent studies; more specifically, these studies focused on the relationship between structural and electronic properties of superlattices of "holes" (termed graphene antidots),[11,14,17,18] chemisorbed atoms,[14,15] and substitutional defects (B and N).[19] These theoretical studies demonstrated that the existence and the width of energy band gaps depend not only on the density of the defects introduced in SLG, but also on their spatial distribution, or more formally, on the symmetry of the resulting superlattice. In cases where the Dirac cones are partially preserved in the resulting band structure, the Fermi velocity also was shown to depend on these symmetry parameters.[14,18,19] The formation of such superstructures allows for a precise control of the electronic properties of graphene, enabling the development of interesting practical applications.

The electronic band structure of pristine twisted bilayer graphene (TBG) resembles that of single-layer graphene and is characterized by the appearance of the Dirac cones (i.e., linear dispersion) in the vicinity of the K point in the first BZ.[20–22] In multilayer graphene, another way of introducing sp^3 bonding and altering the electronic band structure is the formation of interlayer bonds, namely, covalent C-C bonds between atoms of adjacent graphene layers.[16] Several theoretical studies have demonstrated that hydrogenation and formation of such interlayer bonds usually opens a band gap in the electronic band structure;[23–27] again, however, depending on the spatial arrangement of these interlayer bonds, certain features of the electronic band structure of the pristine, nonbonded configuration are preserved.[16] In a recent study[16]

we showed that creation of interlayer C-C bonds in TBG with the individual graphene planes rotated with respect to each other by angles around 30° leads to the formation of superlattices of caged structures (fullerenes) that have the same periodicity with that of the Moiré pattern characteristic of the TBG; depending on the size of these local fullerene structures and the twist angle, the Dirac cones are either preserved or lost opening a narrow gap in the band structure. The effect of interlayer covalent bonding on electron transport in bilayer graphene also has been investigated.[28] Density functional tight binding calculations demonstrated that formation of interlayer C-C bonds in bilayer graphene, resulting from the insertion of atomic defects, leads to a decrease in the electronic conductance of the material but also to significant electronic transport between the layers.[28]

Creation of interlayer C-C bonds also has been studied in multiwalled carbon nanotubes (MWCNTs),[29] aiming at a better understanding of the initial stages of diamond nanostructure formation upon exposure of MWCNTs to a hydrogen plasma, which has been observed experimentally;[30,31] such interlayer bonds generate local nanodomains that resemble bulk diamond structures and can act as seeds for the nucleation of diamond nanocrystals embedded within the MWCNT matrix.[29] This mechanism also may be operative during the synthesis of "diamond nanotubes" (DNTs) by a process the first step of which is the formation of MWCNTs, followed by the appearance of diamond nanostructures.[32]

Previous studies reported structures formed by interlayer bonding in AA- and AB-stacked graphene bilayers,[23–27] as well as in MWCNTs of mixed chirality.[29] In those studies, hydrogen atoms at a surface coverage of 50% were used to passivate dangling bonds at the outer surfaces, being distributed on the surface in a checkerboard pattern; it was shown that the presence of these chemisorbed H atoms stabilized the interlayer-bonded structures. The resulting configurations are characterized by a local crystalline structure that resembles that of diamond; some authors have called them "diamane" or "diamondlike C_2H nanolayer",[24,27] while others have used the terms "hydrogenated bilayer graphene,"[25] "hydrogenated few layer graphene,"[26] or "bilayer graphane".[23] In the study of Ref. 26 it was demonstrated that the energy barriers for the formation of such configurations starting from atomic H and pristine few-layer graphene (FLG) are very low, implying that such structures can be experimentally feasible.

The purpose of this article is to investigate the possible nanostructures that can be formed as a result of covalent interlayer C-C bonding between planes of twisted bilayer graphene based on density functional theory (DFT) calculations. This investigation is carried out over a range of twist angles θ that guarantees the appearance of certain stacking arrangements in TBG. The analysis shows that the resulting structures are superlattices of 2D diamondlike nanocrystalline domains embedded within the graphene planes with a superlattice periodicity equal to that of the TBG Moiré patterns. The formation of such structures impacts the electronic band structure of TBG by either opening a band gap or making TBG metallic. We find that this band gap depends on the density and spatial distribution of interlayer C-C bonds, which introduces parameters that can be used for precise control of band gap tuning in graphene.

The rest of the article is structured as follows. Section II gives a detailed description of the computational methodology employed in our study. In Sec. III we present and discuss the results of our computational analysis, focusing on the atomic and electronic structures of the configurations formed as a result of interlayer C-C bonding within the finite AA- and AB-stacked domains in the unit cell of the TBG superlattice. Finally, the main conclusions and implications of our study are summarized in Sec. IV.

II. COMPUTATIONAL METHODS

DFT calculations were employed for structural relaxation of the generated nanostructures and determination of the electronic band structure of the corresponding relaxed configurations. These calculations were carried out within the local density approximation (LDA)[33] and the generalized gradient approximation (GGA),[34] with plane-wave basis sets for the wave function expansion and ultrasoft pseudopotentials[35] for the representation of the ionic cores as implemented in the QUANTUM ESPRESSO software package.[36] In the GGA calculations we used a dispersion-corrected version of the exchange and correlation functional (PBE-D),[37] which is denoted as GGA-D and includes a semiempirical correction[38] in order to take into account the van der Waals interactions typical of the interlayer interactions in multilayer graphene; the parameters used for the empirical correction of the functional were the same with those suggested in Ref. 37. It has been shown that the use of LDA allows for the accurate prediction of the interlayer spacing c in graphite/graphene bilayers and the correct description of the electronic structure of graphene (both single-layer and multilayered) in the vicinity of the Fermi level, in spite of the LDA's well-known inability to describe long-range dispersion forces.[16,21,22,39,40] Only the Γ point was used for sampling the first BZ in the calculations, employing an energy cutoff of 60 Ry for plane waves and of 540 Ry for charge density. Marzari-Vanderbilt cold smearing[41] was applied with a smearing factor of 0.020 Ry. In the implementation of the supercell approximation, convergence regarding the extent of vacuum used in the direction perpendicular to the graphene planes (distance between images of at least 12 Å) was tested in order to avoid spurious interactions between images. Cell and atomic relaxation were carried out until forces on the atoms reach a tolerance weaker than 0.005 eV/atom. In a limited study of relevant optimal reaction pathways that we conducted, we employed the nudged elastic band (NEB) method[42] in conjunction with DFT calculations for computation of thermal activation energy barriers.

III. RESULTS AND DISCUSSION

A. Atomic structure

The atomic structure of interlayer-bonded configurations in few-layer graphene depends mainly on the local alignment of the atoms in adjacent graphene layers,[16,29] which is defined by the relative displacement of the layers translated or rotated with respect to each other. The two basic patterns for graphene layer stacking are the AA (or hexagonal) stacking, where the atoms of each graphene layer overlap fully when projected to

the graphene plane, and the AB (or Bernal) stacking, where one of the planes in AA stacking is rotated by 60° around the axis normal to the graphene plane or, equivalently, shifted by one C-C bond length in the armchair-oriented direction. In both of these stacking cases, the same local atomic alignment is found throughout the entire domain. When interlayer C-C bonds are created between adjacent graphene planes within AB- and AA-aligned pairs of atoms, two-dimensional (2D) nanostructures are formed resembling the atomic structures of bulk cubic and hexagonal diamond, respectively.[23–27,29]

In TBG, where the two graphene layers are rotated with respect to each other by twist angles θ between 0° and 60°, the honeycomb lattices of each layer generate a superlattice of domains that are characterized by a specific type of local alignment; these superlattices have the same symmetry with but a larger periodicity than the original honeycomb lattice and are called Moiré patterns.[43–46] For twist angles over the range from 0° to ∼16° (or, equivalently, from ∼44° to 60°), these local domains consist of AA- and AB-stacked atoms.[29,44–46] Outside this θ range, qualitatively different stacking patterns are observed, which are similar to the pattern that arises at $\theta = 30°$, where one of the two graphene layers is zigzag oriented and the other one is armchair oriented.[16]

In TBG there is a countably infinite number of twist angles that generates commensurate bilayers; Refs. 47 and 48 give an elegant analytical solution for finding these "magic" angles and the corresponding parameters of the commensurate-bilayer superlattices. In the present study we examined TBG configurations generated by two such twist angles, within the θ range that produces local AA/AB stacking, namely, $\theta = 9.43°$ and $\theta = 13.17°$. The corresponding bilayers are depicted in Fig. 1; the number of C atoms per unit cell of the resulting superlattices is 148 and 76, respectively, with lattice parameters of $\sqrt{111}\ a_{cc}$ and $\sqrt{57}\ a_{cc}$, respectively, where a_{cc} is the sp^2 C-C bond length of the graphene layer. These angles lead to relatively small unit cell sizes, which can be modeled in a computationally efficient manner by DFT within the supercell approximation; similar twist angles also have been observed in TBG samples analyzed in experimental studies.[49–51] The resulting interlayer spacing for the relaxed configurations of these bilayers, as computed by GGA-D, is 3.43 and 3.45 Å for the twist angles of 9.43° and 13.17°, respectively; according to LDA calculations, these interlayer spacings are found to be 3.47 and 3.51 Å, respectively.

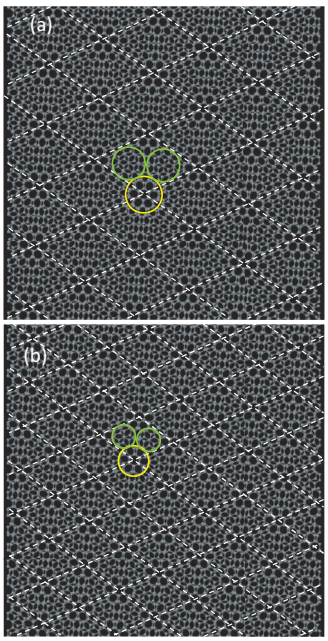

FIG. 1. (Color online) Pristine twisted bilayer graphene with layers rotated with respect to each other by (a) 9.43° and (b) 13.17°. The subdomains marked by light gray (yellow online) and gray (green online) circles correspond to regions of local AA and AB layer stacking, respectively.

Starting from these TBG configurations, we generated interlayer-bonded structures by displacing C atoms of the pristine bilayers in the direction normal to the graphene planes and relaxing the resulting configurations. The atoms selected to be displaced were the ones most likely to participate in the formation of such interlayer C-C bonds, namely, pairs of C atoms (one atom from each graphene layer) that are relatively well aligned in order to minimize the resulting interlayer C-C bond strain.[29] Figure 1 depicts the superlattices of the bilayers investigated with domains characterized by AA and AB stacking; each unit cell of the superlattice contains three such finite domains, one domain of AA-stacked atoms and two domains of AB-stacked atoms. Interlayer C-C bonds were created within these domains, generating superlattices of 2D diamondlike structures embedded within the two graphene layers of the original TBG.

We investigated numerous relaxed interlayer-bonded configurations containing different numbers of interlayer bonds per unit cell N_{IB} ranging from a single interlayer C-C bond to the maximum possible number of such bonds allowed per unit cell; in each case, this maximum N_{IB} value depends on the size of the locally aligned domains, which decreases with increasing twist angle θ.[29,46] Figures 2–4 show different views of the supercells used in the calculations; in the depicted structures the atoms that participate in interlayer C-C bonding and the formed C-C bonds are shaded light gray (colored orange online). Hydrogen atoms were chemisorbed onto each graphene layer at every C atom that is a nearest neighbor of a C atom involved in the interlayer bonding; these hydrogenated interlayer-bonded configurations were found to be the thermodynamically most stable ones. In general, the presence of hydrogen atoms (or some other functionalizing agent) is of major importance for stabilizing the C-C interlayer bonds formed.[16,23]

In order to define and characterize the generated interlayer-bonded configurations, three parameters are required: the twist angle θ, the local layer stacking type st, and the number of interlayer C-C bonds per unit cell of the superlattice N_{IB}, that is, each configuration is determined by the triplet (θ, st, N_{IB}). Therefore, the resulting structures for the bilayers with $\theta = 9.43°$ and $\theta = 13.17°$ are denoted as (9.43°, st, N_{IB}) and (13.17°, st, N_{IB}), respectively, where st = AA, AB, AAAB, or ABAB depending on the local stacking of atoms that participate in the interlayer C-C bonding that generates the N_{IB} such bonds; st = AAAB means that the interlayer C-C bonds are formed within both AA- and AB-stacked domains in the unit cell and st = ABAB means that these bonds are formed within both of the two AB-stacked domains in the unit

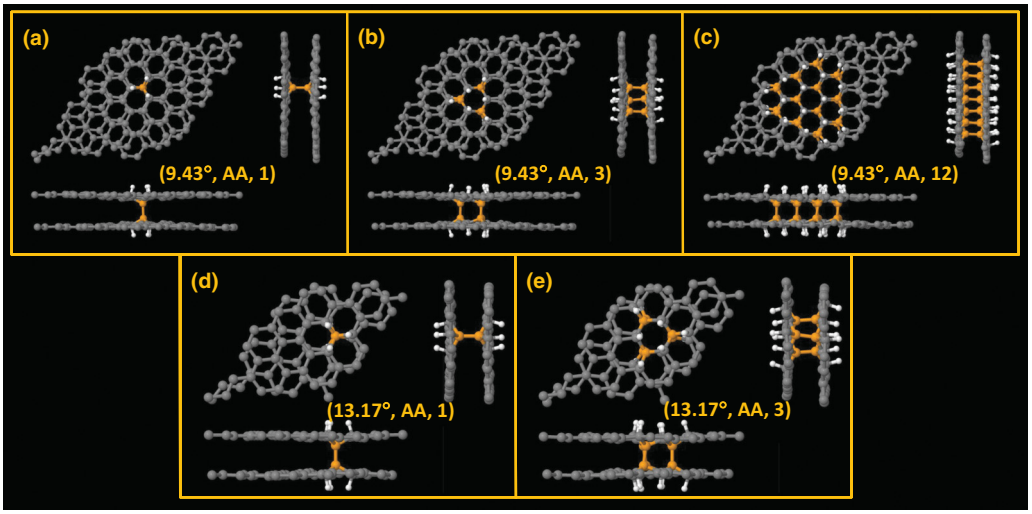

FIG. 2. (Color online) Supercells of (hexagonal) diamond nanodomains embedded in TBG, consisting of various interlayer-bonded configurations with interlayer C-C bonds created in regions of AA layer stacking with graphene layers rotated with respect to each other by (a–c) 9.43° and (d, e) 13.17°. Each panel shows top (upper-left corner) and side (upper-right and bottom corners) views of the configurations.

cell. Figures 2 and 3 show interlayer-bonded configurations where C-C bonds are formed within only AA-stacked and only one AB-stacked domain in the unit cell, respectively. Figure 4 shows configurations where interlayer C-C bonds are formed simultaneously within both AA- and AB-stacked domains (st = AAAB), or within different locally AB-stacked domains within the same supercell (st = ABAB).

In order to check the relative thermodynamic stability of the generated interlayer-bonded configurations, we computed the formation energy E_f of each one of them, defined as $E_f = (E_{\mathrm{IBS}} - E_{\mathrm{TBG}} - N_{\mathrm{H}}E_{\mathrm{H}})/(N_{\mathrm{H}} + N_{\mathrm{C}})$, where E_{IBS} is the energy of the interlayer-bonded structure, E_{TBG} is the energy of the pristine twisted bilayer that gave origin to the interlayer-bonded configuration, E_{H} is the energy of an isolated hydrogen atom, and N_{H} and N_{C} are the total numbers of hydrogen and carbon atoms in the configuration under consideration. The calculated formation energies as a function of N_{IB} are given in Fig. 5(a), as predicted by the GGA-D calculations; LDA calculations yielded the same trend for $E_f(N_{\mathrm{IB}})$, with slightly lower (by 3 to 20 meV/atom) values for the actual energies. In all the cases examined, $E_f < 0$, indicating that the interlayer bonded structures are thermodynamically stable with respect to the reference state used in the E_f definition, consisting of pristine TBG and atomic hydrogen. This suggests that such configurations can be observed experimentally upon exposure of the TBG surfaces to a flux of atomic hydrogen, which can be generated, for example, by a H_2 plasma. The results of Fig. 5(a) indicate that E_f increases with increasing N_{IB}; however, the average decrease in the total energy per interlayer C-C bond introduced, E_f/N_{IB}, decreases with increasing N_{IB}, as shown in Fig. 5(b). These results imply that the growth of such interlayer-bonded domains is favorable from one interlayer bond up to the maximum allowed domain size, determined by the maximum allowed N_{IB}.

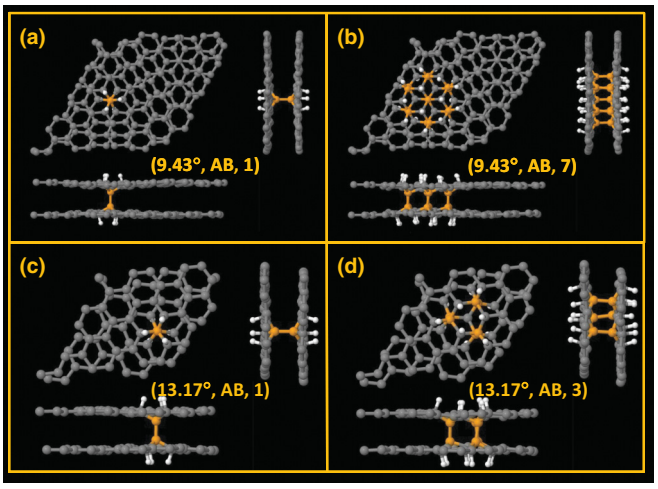

FIG. 3. (Color online) Supercells of (cubic) diamond nanodomains embedded in TBG, consisting of various interlayer-bonded configurations with interlayer C-C bonds created in regions of AB layer stacking with graphene layers rotated with respect to each other by (a, b) 9.43° and (c, d) 13.17°. Each panel shows top (upper-left corner) and side (upper-right and bottom corners) views of the configurations.

Although the investigation of interlayer C-C bond formation mechanisms and determination of the corresponding energy barriers are not within the scope of this study, we discuss briefly the stability of these hydrogenated interlayer-bonded structures against the eventual detachment of the two layers from each other or hydrogen desorption from the surfaces. For the 2D interlayer-bonded structures formed from AB-stacked layers at $\theta = 0°$ and at the maximum N_{IB},[23–27] that is, for continuous 2D diamond structures, the energy barrier required to break the interlayer bonds and separate the two graphene layers is ∼5 eV[26] according to DFT/GGA calculations; this energy barrier is practically equal to the energy difference between the interlayer-bonded and nonbonded states. Consequently, for the interlayer-bonded nanostructures of Figs. 2–4, the energy per bond required to break the interlayer bonds must be comparable to ∼5 eV even

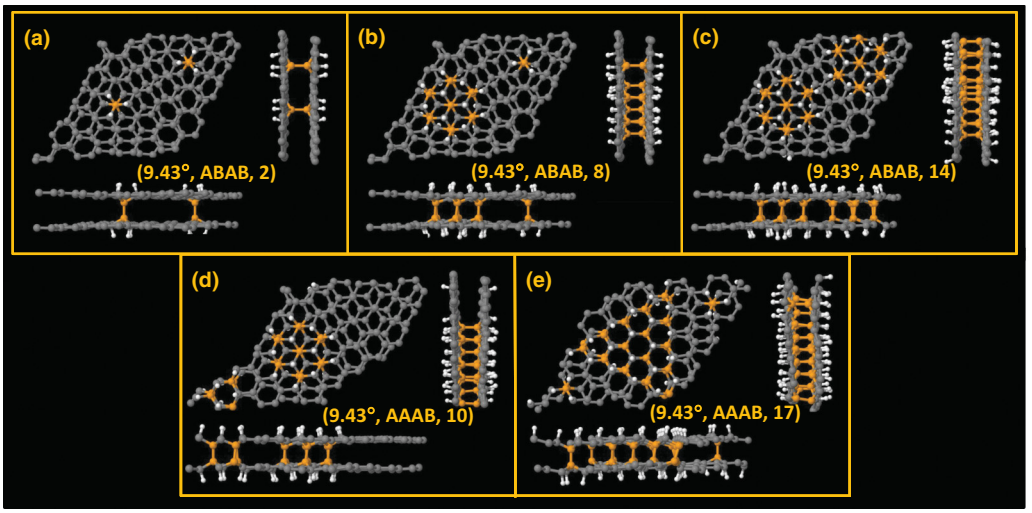

FIG. 4. (Color online) Supercells of diamond nanodomains embedded in TBG, consisting of various interlayer-bonded configurations with interlayer C-C bonds created in regions of (a–c) AB and (d, e) both AB and AA layer stacking with graphene layers rotated with respect to each other by 9.43°. Each panel shows top (upper-left corner) and side (upper-right and bottom corners) views of the configurations.

though the number of interlayer bonds per unit cell N_{IB} is lower than that of the continuous 2D diamond domains.

Experimental studies have demonstrated that the hydrogenation of graphene and graphite and the formation of graphane are reversible processes;[4,5,52,53] at high temperatures, over the range from 600 to 1073 K, H atoms chemisorbed onto hydrogenated graphene/graphite layers diffuse on the surface and recombine to form and release H_2 molecules.[52] A similar response is expected for the interlayer-bonded structures examined in this study due to their chemical similarity with graphane; both types of structure correspond to a hydrogenated 2D sp^3-bonded carbon network.

DFT/GGA calculations[54] have shown that the energy barrier for recombination and desorption of H_2 from pure graphane in the chair configuration is ∼4.3 eV; this configuration is structurally analogous to the core of our interlayer-bonded domains. For graphane/graphene interfaces (with structure analogous to that of the boundary between our interlayer-bonded domains and bilayer graphene), this energy lies within the range from ∼1.0 to 4.2 eV.[54] Due to their chemical and structural similarity with the above configurations, it is expected that the interlayer-bonded structures examined here will be at least as stable as graphane at high temperature; this makes our interlayer-bonded structures suitable for applications under typical thermal conditions. A comprehensive analysis of the barriers for H_2 desorption from the interlayer-bonded structures of this study also is beyond the scope of this article. To simply approximate the magnitude of these barriers, we employed DFT calculations in conjunction with the NEB method to compute the energy barrier for desorption of H_2 from graphane in the chair configuration and from interlayer bonded AA- and AB-stacked bilayers that yield continuous 2D diamond structures using 2 × 2 supercells. We found that all of these energies are of comparable level and equal to 4.6, 5.0, and 4.8 eV, respectively. These results support the expectation that our interlayer-bonded structures are as stable as graphane.

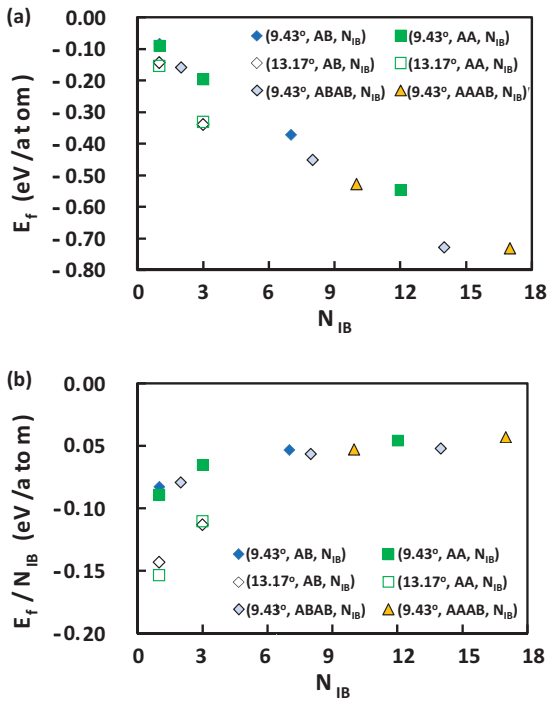

FIG. 5. (Color online) (a) Formation energy E_f and (b) formation energy per number of interlayer C-C bonds E_f/N_{IB} of the superstructures of diamond nanodomain configurations embedded in TBG as a function of the number of interlayer C-C bonds per unit cell N_{IB}.

B. Electronic structure

Based on DFT calculations, as described in Sec. II, we determined the electronic band structures of the twisted bilayers in their pristine state and of the hydrogenated interlayer-bonded configurations presented and discussed in Sec. III A.

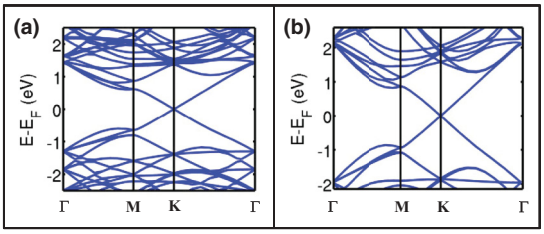

FIG. 6. (Color online) Electronic band structure of pristine twisted bilayer graphene with a twist angle of (a) 9.43° and (b) 13.17°.

The results are summarized in Figs. 6–9. These results were obtained by using the GGA-D exchange and correlation functional; predictions based on LDA are essentially the same with those reported in Figs. 6–9, with only some slight quantitative differences in the energy predictions, as seen in Table I. In all cases, the corresponding dispersion relations are plotted along the path Γ-M-K-Γ that connects these three special points in the first BZ of the supercell. Curves are shifted in the vertical direction in order to make the Fermi level E_F coincide with a zero energy level exactly midway between the top of the valence band and the bottom of the conduction band. Figure 6 shows that, as expected, the electronic structure of pristine nonbonded TBG preserves the Dirac cones at the K point, which is typical of the band structure of single-layer graphene,[20–22] due to the electronic decoupling of the two graphene layers.

The band structures of the interlayer-bonded configurations generated from AA- and AB-stacked bilayers that yield continuous 2D diamond structures have been reported in the literature; they have been found to be insulators, with band gaps over the range from 2.5 to 3.5 eV as predicted by DFT calculations within the GGA approximation.[23–27] We also carried out electronic band structure calculations for some of these same reported atomic structures, following the procedure described in Sec. II; our results were in excellent agreement with the published DFT predictions.

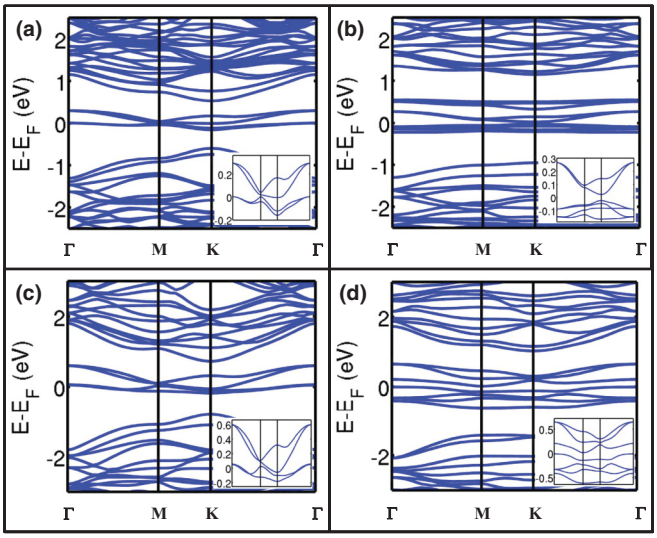

FIG. 8. (Color online) Electronic band structures of superlattices of diamond nanodomains embedded in TBG, consisting of various interlayer-bonded configurations with interlayer C-C bonds created in AB-stacked regions of the unit cell. The parameters (θ, st, N_{IB}) of the corresponding atomic configurations are (a) (9.43°, AB, 1), (b) (9.43°, AB, 7), (c) (13.17°, AB, 1), and (d) (13.17°, AB, 3). Each inset highlights the dispersion relation in the vicinity of the Fermi level and the opening (or not) of a band gap.

The hydrogenated interlayer-bonded structures introduced in the present study are characterized by the presence of both sp^2- and sp^3-hybridized C-C bonds, which has significant effects on the resulting electronic band structure. When interlayer bonds are created within AA-aligned regions in TBG (as done in the configurations of Fig. 2), the Dirac

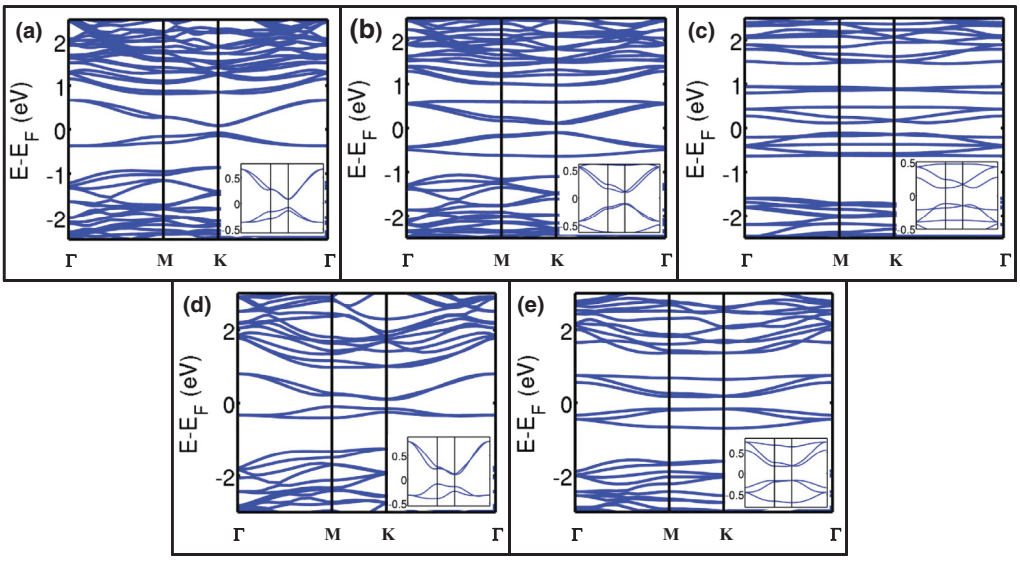

FIG. 7. (Color online) Electronic band structures of superlattices of diamond nanodomains embedded in TBG, consisting of various interlayer-bonded configurations with interlayer C-C bonds created in AA-stacked regions of the unit cell. The parameters (θ, st, N_{IB}) of the corresponding atomic configurations are (a) (9.43°, AA, 1), (b) (9.43°, AA, 3), (c) (9.43°, AA, 12), (d) (13.17°, AA, 1), and (e) (13.17°, AA, 3). Each inset highlights the dispersion relation in the vicinity of the Fermi level and the opening of a band gap.

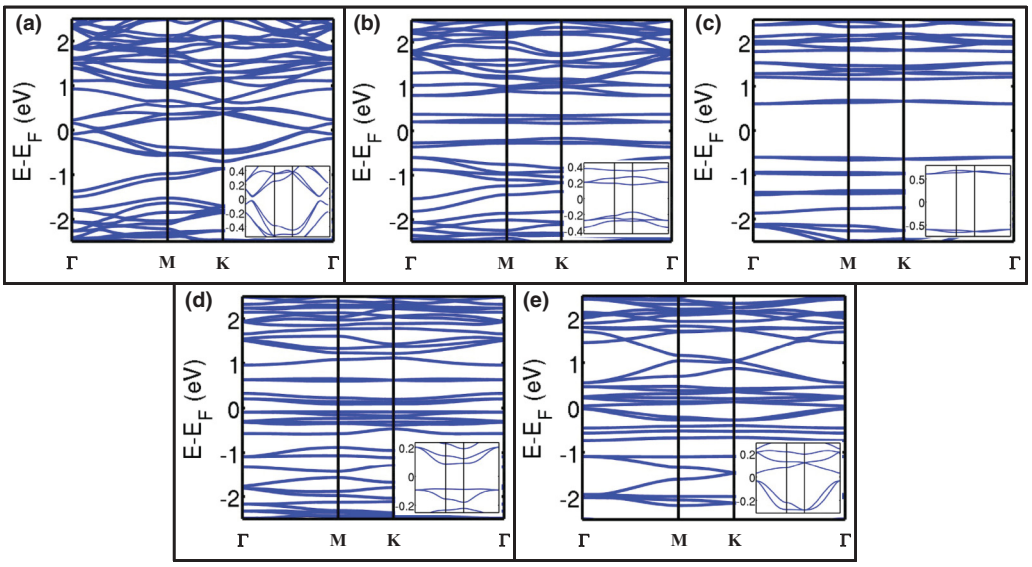

FIG. 9. (Color online) Electronic band structures of superlattices of diamond nanodomains embedded in TBG, consisting of various interlayer-bonded configurations with interlayer C-C bonds created in two different AB-stacked or both AB- and AA-stacked regions of the unit cell. The parameters (θ, st, N_{IB}) of the corresponding atomic configurations are (a) (9.43°, ABAB, 2), (b) (9.43°, ABAB, 8), (c) (9.43°, ABAB, 14), (d) (9.43°, AAAB, 10), and (e) (9.43°, AAAB, 17). Each inset highlights the dispersion relation in the vicinity of the Fermi level and the opening of a band gap.

cones at the K point disappear and a band gap is opened, as depicted in Fig. 7; the size of this band gap E_g depends on the number of interlayer bonds per unit cell N_{IB} or, equivalently, on the fraction of sp^3-bonded C atoms in the atomic configuration. In this case, a hexagonal superlattice of interlayer-bonded domains is generated, with the point-group symmetry (originally D_{6h}, characteristic of single-layer graphene) being reduced to D_{3h}, and a band gap opening is expected.[14,19] The dependence of the band gaps on N_{IB} is analogous to the case of graphene antidots, where given a superlattice periodicity and symmetry, increasing the size of the holes typically increases the band gap.[11,14,17] Figure 10 shows the dependence of E_g on N_{IB} for the hydrogenated interlayer-bonded structures we generated. When interlayer bonds are created within AB-aligned regions (as in the configurations of Fig. 3), the corresponding band structures, depicted in Fig. 8, indicate that the resulting atomic structure exhibits metallic behavior at $N_{IB} = 1$; however, a band gap is opened, with increasing N_{IB}. Figure 9 shows the band structures of configurations (such as those of Fig. 4), where interlayer C-C bonds are created within different subdomains in the same supercell, that is, for st = AAAB or ABAB, resulting in hexagonal and honeycomb superlattices and also in a larger density of interlayer bonds (higher N_{IB}); in this case, wider band gaps open for some configurations, while for others the band gaps are comparable to those in Figs. 7 and 8.

Even though it is well known that DFT underestimates electronic band gaps as compared to experimental results, the $E_g(N_{IB})$ trend presented in Fig. 10 is clear. The computed

TABLE I. Comparison between computed band gaps (in eV) of the generated interlayer-bonded structures according to DFT/GGA-D and DFT/LDA calculations. "NC" is used to denote that the energy gap was not computed using the corresponding approximation.

Configuration	E_g (GGA-D/LDA)
(9.43°, AB, 1)	metallic/metallic
(9.43°, AB, 7)	0.05/0.08
(9.43°, AA, 1)	0.16/0.17
(9.43°, AA, 3)	0.20/0.21
(9.43°, AA, 12)	0.23/0.24
(9.43°, ABAB, 2)	0.05/NC
(9.43°, ABAB, 8)	0.34/NC
(9.43°, ABAB, 14)	1.21/NC
(9.43°, AAAB, 10)	0.17/NC
(9.43°, AAAB, 17)	0.06/NC
(13.17°, AB, 1)	metallic/metallic
(13.17°, AB, 3)	0.02/metallic
(13.17°, AA, 1)	0.20/0.19
(13.17°, AA, 3)	0.33/0.35

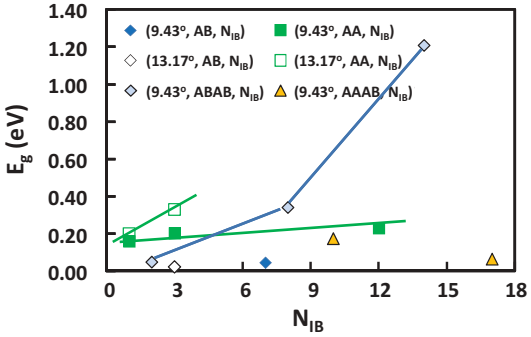

FIG. 10. (Color online) Electronic band gap E_g of the superstructures of diamond nanodomain configurations embedded in TBG as a function of the number of interlayer C-C bonds per unit cell N_{IB} for various values of the parameters θ and st. The drawn lines simply provide a guide to the eye.

band gaps for the hydrogenated interlayer-bonded structures that we generated and analyzed range from a few meV up to ∼1.2 eV. Importantly, for a given superlattice symmetry and periodicity, E_g is seen to increase with increasing N_{IB}, that is, the higher the density of interlayer C-C bonds, the wider the opening of the band gap. This monotonic increase of E_g with N_{IB} implies that the formation of such nanostructures can be used to open a tunable band gap in graphene in a precisely controlled fashion, using as control parameters the symmetry of the superlattice and the density of the formed sp^3 interlayer bonds, that is, the size, shape, and spatial distribution of the 2D diamond nanodomains generated by the interlayer C-C bonding, as expressed by the corresponding triplet of degrees of freedom (θ, st, N_{IB}). The same fine tuning of electronic properties demonstrated by creating superlattices of defects in SLG[11,14,15,17–19] can be accomplished by the superlattices of finite 2D diamondlike clusters introduced in the present study. Our nanodiamond superlattices, as well as the superlattices reported in Ref. 16, are conceptually analogous to the SLG-based defect superlattices, with one fundamental difference: these 2D superstructures originate from twisted bilayer graphene (TBG) instead of single-layer graphene. This difference in the superlattice structure, as well as the local atomic structure due to the interlayer C-C bonding, may endow these TBG-based nanomaterials with distinct (chemical, mechanical, structural, and morphological) properties when compared to single-layered configurations; this is a topic that deserves to be explored further.

The existence of such diverse features in the electronic band structure is a result of the chemical nature of the superlattices of interlayer-bonded configurations that we formed. The introduction of sp^3 C-C bonds, through H chemisorption and formation of covalent interlayer bonds, creates defects in the network of delocalized sp^2 C-C bonds, opening a band gap in the electronic band structure.[4–8,12] Depending on the density of interlayer bonds and of hydrogenated sites, and on how they are distributed on the graphene layer, conjugated sp^2 bonding can be partially preserved in these configurations, leading to conducting π bands.[14–16] Confinement of electrons within finite sp^2-bonded domains of modified graphene can lead to semiconducting or metallic behavior depending on the size and geometry of these domains.[55]

In general, increasing the number of interlayer covalent bonds (or any defects in the network of delocalized sp^2 C-C bonds) would be expected to intensify the effect of defects on the electronic structure and, consequently, increase the band gap, as observed in most of our results in Fig. 10. However, it is possible to form large diamond domains in such interlayer-bonded structures that preserve conjugated sp^2 bonds, as is the case for configurations with parameters (9.43°, AAAB, 10) and (9.43°, AAAB, 17); in spite of the high N_{IB} values of these structures, the resulting band gaps are comparable to those with lower interlayer bond densities. The opposite behavior is observed for the configuration with parameters (9.43°, ABAB, 14); in this case, the nanocrystalline diamond domains break the network of conjugated sp^2 bonding, confining electrons within domains of unmodified graphene (here, more specifically, within the AA-stacked regions) and, as a result, opening a wide band gap in the electronic band structure. Similar behavior has been demonstrated for superstructures of antidot lattices,[11,14,15,17,18] where the resulting band gap was found to depend not only on the size of the "holes" in the structure, but also on the specific geometry and symmetry of the superlattice and, consequently, in the presence of a delocalized sp^2 bonding network. Also, it must be emphasized that for the (9.43°, ABAB, 14) configuration, a honeycomb superlattice analogous to the ones studied in Ref. 14 is generated; the study of Ref. 14 has demonstrated that due to their particular symmetry, these configurations lead to the widest band gaps per number of defects introduced.

These features also explain why the band gaps exhibited by the interlayer-bonded structures introduced in this study are considerably narrower than the ones exhibited by the interlayer-bonded continuous 2D diamond structures generated in AA- or AB-stacked graphene bilayers that range from 2.5 to 3.5 eV.[23–27] In these 2D diamond configurations, the structure is formed exclusively by sp^3-hybridized C-C bonds, which are responsible for the insulating nature of these nanomaterials as they are for that of bulk cubic diamond.

The opening of a band gap due to formation of covalently bonded domains embedded within graphene layers has been demonstrated in experimental studies, but in different contexts. Experimental studies of adsorption of H atoms onto graphene supported by Ir(111) substrates have shown that hydrogen adsorbs onto the substrate surface selectively[6]: As a consequence of the Moiré patterns resulting from the superposition of the graphene layers onto the metallic surface, "graphane islands" are arranged in a superlattice throughout the surface. There are specific regions where every other carbon atom from the graphene layer is perfectly aligned with an Ir atom from the substrate; this leads to formation of covalent bonds between C and Ir atoms in an alternate pattern; followed by chemisorption of H atoms onto the neighboring C atoms, this generates a superlattice of graphanelike local structures. These experiments, in conjunction with calculations, demonstrated that a band gap is opened in these structures and that this band gap depends on the degree of hydrogenation and, consequently, on the size of the covalently bonded domains.[6] Another recent experimental study[56] investigated the effect of chemical fusion of presynthesized nanodiamond particles to a graphene matrix on the graphene's electronic and magnetic properties; as expected, the electronic properties are affected in the same way that was discussed above, as observed by an increase in the conduction resistance of the graphene sheets after the binding of the nanoparticles.

IV. SUMMARY AND CONCLUSIONS

We have carried out a first-principles computational analysis of superlattice formation of diamond nanocrystalline domains embedded in twisted bilayer graphene. These superstructures have the periodicity of the underlying Moiré pattern and are formed upon creation of covalent interlayer C-C bonds in domains of the graphene bilayer characterized by AA and AB stacking over a range of twist angles from 0° to about 15°. The formation of these interlayer bonds alters the electronic band structure of the original nonbonded bilayer by usually opening a band gap, which can be tuned by controlling the embedded nanodomain sizes, that is, the density and spatial distribution of the formed interlayer C-C bonds. As discussed

in Sec. III B, formation of defect superlattices in graphene (both single-layer graphene[11,14,15,17–19] and, in the present case and that of Ref. 16, twisted bilayer graphene) are promising alternatives for the fine tuning of its electronic properties, enabling the development of various practical applications. For our nanodiamond superstructures we found energy gaps of the same order of magnitude as those reported for the SLG-based defect superlattices in previous studies.[11,14,15,17–19] Therefore, the present study demonstrates that numerous opportunities may remain to be explored in the formation of superstructures based on single-layer and few-layer graphene materials that may introduce new nanomaterials with unique properties and function.

The computed formation energies reported in Sec. III A imply that the embedded nanodiamond superstructures studied in this work are experimentally feasible and can be synthesized starting from twisted bilayer graphene and exposing it to atomic hydrogen according to proper experimental protocols to generate the required hydrogenation patterns. Formation of interlayer C-C bonds in graphitic materials can be induced by high pressure/temperature or shock compression, which can cause a graphite-to-diamond structural transition.[57–59] Theoretical studies also have shown that interlayer C-C covalent bonds can be formed as a result of a healing mechanism when defects are introduced in multilayered carbon materials,[28,60,61] for example, due to ion/electron irradiation. Indeed, synthesis of diamond nanocrystals starting from graphitic materials has been achieved in a series of irradiation experiments; one well known example is the transformation of carbon onions (concentric-shell, onionlike graphitic structures) into nanodiamond, by exposure to an electron beam at temperatures over the range from 600 to 1000 K.[62,63] Another means of such interlayer C-C bond formation, already mentioned in Sec. I, is the exposure of MWCNTs to atomic hydrogen fluxes, which leads to formation of diamond nanocrystals embedded within the graphene walls of the MWCNTs.[29–31]

Recent experimental studies have demonstrated the possibility of selective hydrogenation of graphene[53] leading to atomic H chemisorption onto specified regions of the graphene plane; such experimental techniques could be applied to tailor the distribution of H atoms on the outer surfaces of the graphene planes in TBG during or before inducing the formation of the interlayer C-C bonds. The thermodynamics and kinetics of formation of the embedded nanodiamond superstructures reported in this article is well beyond the scope of the present study. We mention, however, that a previous study[26] has demonstrated that the activation energy barriers associated with the formation of such interlayer-bonded nanostructures, starting from atomic H and pristine AB-stacked few-layer graphene, are quite low, which also implies that synthesis of such structures is indeed experimentally feasible.

It was demonstrated in Sec. III B that the creation of diamond nanodomains due to interlayer C-C bonding in TBG provides a systematic approach for the precise tuning of the band gap of graphene reaching band gaps wider than 1 eV. The computational demand for the first-principles DFT calculations employed in this work limited our investigation to relatively small supercells (up to 154 C atoms) that correspond to relatively high values of the twist angle θ; this, in turn, has limited the size range of the interlayer-bonded domains examined in this study. For smaller twist angles, larger-size diamond nanocrystals can be formed by interlayer C-C bonding, resulting in potentially wider band gaps than those reported in this article; more importantly, this can lead to more precise control of the interlayer-bond density and, consequently, finer tuning of the band gap.

In order to explore the entire set of physical properties, including thermal, optical, and magnetic properties, exhibited by this class of nanostructures, further theoretical analysis needs to be carried out. The findings of such theoretical studies will allow for a comprehensive evaluation of the potential of such graphene-based nanodiamond superstructures for a range of technological applications, and also to verify which technical advantages they would present when compared to other graphene-derived materials, such as graphane[4–7,13] and other classes of defect superlattices.[11,14,15,17–19] As discussed in Sec. III B, it is expected that this new class of nanomaterials is endowed by properties "inherited" from each one of its constituents: sp^2-hybridized domains of graphene in TBG and sp^3-hybridized nanodiamond domains; analogous behavior has been reported for nanostructures with similar structural and chemical features.[6,56]

The surface reactivity of such interlayer-bonded graphene-based nanomaterials also is worth exploring. For example, it is well known that sp^3-hybridized C atoms are more reactive than sp^2-hybridized C atoms when exposed to free radicals.[56] Moreover, we know that after the chemisorption of one H atom on a graphene plane, the chemisorption of a second H atom can be barrierless depending on the adsorption site.[64] Pristine graphene is harder to functionalize; typically, covalent bonds are easier to form at the graphene layer edges, ripples, and structural defects.[65] The sp^3 character introduced by the diamondlike nanocrystals embedded within the graphene layers of TBG make the graphene surfaces easier to functionalize further with other species, as demonstrated experimentally in patterned superlattices of hydrogenated sites on graphene.[53] Diamond nanocrystals have been functionalized with a series of species, aiming at different types of applications.[66] Diamond nanodomains and other nanostructures embedded in the TBG bilayer could serve as a platform for the creation of hybrid nanomaterials with the interlayer-bonded domains providing the "anchors" for attachment of new species. One major advantage of this approach is the capability of creating ordered superlattice structures templated on the TBG's Moiré pattern. Such structures also may be used to attach diamond nanocrystals directly to the graphene layer, providing an alternative to the experimental procedure of Ref. 56, or to induce growth of larger domains of crystalline diamond protruding from the graphene layers, similar to what has been observed in carbon nanotubes.[30,31]

ACKNOWLEDGMENTS

A.R.M. acknowledges CESUP/UFRGS for using their computational facility and FAPERGS for travel Grant No. 11/3445-5. D.M. acknowledges support by Polymer-Based Materials for Harvesting Solar Energy, an Energy Frontier Research Center funded by the US Department of Energy (DOE), Office of Basic Energy Sciences under Award No. DE-SC0001087.

*Corresponding author: maroudas@ecs.umass.edu

[1] K. S. Novoselov, A. K. Geim, S. V. Morozov, D. Jiang, Y. Zhang, S. V. Dubonos, I. V. Grigorieva, and A. A. Firsov, Science **306**, 666 (2004).

[2] A. K. Geim, Science **324**, 1530 (2009).

[3] A. H. Castro Neto, F. Guinea, N. M. R. Peres, K. S. Novoselov, and A. K. Geim, Rev. Mod. Phys. **81**, 109 (2009).

[4] D. C. Elias, R. R. Nair, T. M. G. Mohiuddin, S. V. Morozov, P. Blake, M. P. Halsall, A. C. Ferrari, D. W. Boukhvalov, M. I. Katsnelson, A. K. Geim, and K. S. Novoselov, Science **323**, 610 (2009).

[5] R. Balog, B. Jørgensen, J. Wells, E. Lægsgaard, P. Hoffmann, F. Besenbacher, and L. Hornekær, J. Am. Chem. Soc. **131**, 8744 (2009).

[6] R. Balog, B. Jørgensen, L. Nilsson, M. Andersen, E. Rienks, M. Bianchi, M. Fanetti, E. Lægsgaard, A. Baraldi, S. Lizzit, Z. Sljivancanin, F. Besenbacher, B. Hammer, T. G. Pedersen, P. Hofmann, and L. Hornekær, Nat. Mater. **9**, 315 (2010).

[7] R. R. Nair, W. Ren, R. Jalil, I. Riaz, V. G. Kravets, L. Britnell, P. Blake, F. Schedin, A. S. Mayorov, S. Yuan, M. I. Katsnelson, H.-M. Cheng, W. Strupinski, L. G. Bulusheva, A. V. Okotrub, I. V. Grigorieva, A. N. Grigorenko, K. S. Novoselov, and A. K. Geim, Small **6**, 2877 (2010).

[8] S. Niyogi, E. Bekyarova, J. Hong, S. Khizroev, C. Berger, W. de Heer, and R. C. Haddon, J. Phys. Chem. Lett. **2**, 2487 (2011).

[9] M. Y. Han, B. Ozyilmaz, Y. Zhang, and P. Kim, Phys. Rev. Lett. **98**, 206805 (2007).

[10] E. V. Castro, K. S. Novoselov, S. V. Morozov, N. M. R. Peres, J. M. B. Lopes dos Santos, J. Nilsson, F. Guinea, A. K. Geim, and A. H. Castro Neto, Phys. Rev. Lett. **99**, 216802 (2007).

[11] T. G. Pedersen, C. Flindt, J. Pedersen, N. A. Mortensen, A.-P. Jauho, and K. Pedersen, Phys. Rev. Lett. **100**, 136804 (2008).

[12] E. J. Duplock, M. Scheffler, and P. J. D. Lindan, Phys. Rev. Lett. **92**, 225502 (2004).

[13] J. O. Sofo, A. S. Chaudhari, and G. D. Barber, Phys. Rev. B **75**, 153401 (2007).

[14] R. Martinazzo, S. Casolo, and G. F. Tantardini, Phys. Rev. B **81**, 245420 (2010).

[15] J. M. García-Lastra, Phys. Rev. B **82**, 235418 (2010).

[16] A. R. Muniz and D. Maroudas, J. Appl. Phys. **111**, 043513 (2012).

[17] R. Petersen, T. G. Pedersen, and A.-P. Jauho, ACS Nano **5**, 523 (2011).

[18] F. Ouyang, S. Peng, Z. Liu, and Z. Liu, ACS Nano **5**, 4023 (2011).

[19] S. Casolo, R. Martinazzo, and G. F. Tantardini, J. Phys. Chem. C **115**, 3250 (2011).

[20] J. M. B. Lopes dos Santos, N. M. R. Peres, and A. H. Castro Neto, Phys. Rev. Lett. **99**, 256802 (2007).

[21] S. Latil, V. Meunier, and L. Henrard, Phys. Rev. B **76**, 201402(R) (2007).

[22] J. Hass, F. Varchon, J. E. Millan-Otoya, M. Sprinkle, N. Sharma, W. A. de Heer, C. Berger, P. N. First, L. Magaud, and E. H. Conrad, Phys. Rev. Lett. **100**, 125504 (2008).

[23] O. Leenaerts, B. Partoens, and F. M. Peeters, Phys. Rev. B **80**, 245422 (2009).

[24] L. A. Chernozatonskii, P. B. Sorokin, A. G. Kvashnin, and D. G. Kvashnin, JETP Lett. **90**, 134 (2009).

[25] D. K. Samarakoon and X.-Q. Wang, ACS Nano **4**, 4126 (2010).

[26] L. Zhu, H. Hu, Q. Chen, S. Wang, J. Wang, and F. Ding, Nanotechnology **22**, 185202 (2011).

[27] L. A. Chernozatonskii, P. B. Sorokin, A. A. Kuzubov, B. P. Sorokin, A. G. Kvashnin, D. G. Kvashnin, P. V. Avramov, and B. I. Yakobson, J. Phys. Chem. C **115**, 132 (2011).

[28] E. Cruz-Silva, A. R. Botello-Méndez, Z. M. Barnett, X. Jia, M. S. Dresselhaus, H. Terrones, M. Terrones, B. G. Sumpter, and V. Meunier, Phys. Rev. Lett. **105**, 045501 (2010).

[29] A. R. Muniz, T. Singh, E. S. Aydil, and D. Maroudas, Phys. Rev. B **80**, 144105 (2009).

[30] L. T. Sun, J. L. Gong, Z. Y. Zhu, D. Z. Zhu, S. X. He, Z. X. Wang, Y. Chen, and G. Hu, Appl. Phys. Lett. **84**, 2901 (2004).

[31] L. Sun, J. Gong, Z. Zhu, D. Zhu, and S. He, Adv. Mater. **16**, 1849 (2004).

[32] D. Varshney, V. I. Makarov, P. Saxena, J. F. Scott, B. R. Weiner, and G. Morell, Europhys. Lett. **95**, 28002 (2011).

[33] J. P. Perdew and A. Zunger, Phys. Rev. B **23**, 5048 (1981).

[34] J. P. Perdew, K. Burke, and M. Ernzerhof, Phys. Rev. Lett. **77**, 3865 (1996).

[35] D. Vanderbilt, Phys. Rev. B **41**, 7892 (1990).

[36] P. Giannozzi, S. Baroni, N. Bonini, M. Calandra, R. Car, C. Cavazzoni, D. Ceresoli, G. L. Chiarotti, M. Cococcioni, I. Dabo, A. Dal Corso, S. de Gironcoli, S. Fabris, G. Fratesi, R. Gebauer, U. Gerstmann, C. Gougoussis, A. Kokalj, M. Lazzeri, L. Martin-Samos, N. Marzari, F. Mauri, R. Mazzarello, S. Paolini, A. Pasquarello, L. Paulatto, C. Sbraccia, S. Scandolo, G. Sclauzero, A. P. Seitsonen, A. Smogunov, P. Umari, and R. M. Wentzcovitch, J. Phys.: Condens. Matter **21**, 395502 (2009).

[37] V. Barone, M. Casarin, D. Forrer, M. Pavone, M. Sambi, and A. Vittadini, J. Comput. Chem. **30**, 934 (2009).

[38] S. Grimme, J. Comput. Chem. **27**, 1787 (2006).

[39] S. Latil and L. Henrard, Phys. Rev. Lett. **97**, 036803 (2006).

[40] M. Aoki and H. Amawashi, Solid State Commun. **142**, 123 (2007).

[41] N. Marzari, D. Vanderbilt, A. De Vita, and M. C. Payne, Phys. Rev. Lett. **82**, 3296 (1999).

[42] G. Henkelman, B. P. Uberuaga, and H. Jonsson, J. Chem. Phys. **113**, 9901 (2000).

[43] M. Kuwabara, D. R. Clarke, and D. A. Smith, Appl. Phys. Lett. **56**, 2396 (1990).

[44] J. Xhie, K. Sattler, M. Ge, and N. Venkateswaran, Phys. Rev. B **47**, 15835 (1993).

[45] Z. Y. Rong and P. Kuiper, Phys. Rev. B **48**, 17427 (1993).

[46] J. M. Campanera, G. Savini, I. Suarez-Martinez, and M. I. Heggie, Phys. Rev. B **75**, 235449 (2007).

[47] S. Shallcross, S. Sharma, and O. A. Pankratov, Phys. Rev. Lett. **101**, 056803 (2008).

[48] S. Shallcross, S. Sharma, E. Kandelaki, and O. A. Pankratov, Phys. Rev. B **81**, 165105 (2010).

[49] F. Varchon, P. Mallet, L. Magaud, and J.-Y. Veuillen, Phys. Rev. B **77**, 165415 (2008).

[50] J. H. Warner, M. H. Rummeli, T. Gemming, B. Buchner, and G. A. D. Briggs, Nano Lett. **9**, 102 (2009).

[51] J. Hass, W. A. de Heer, and E. H. Conrad, J. Phys.: Condens. Matter **20**, 323202 (2008).

[52] L. Hornekær, Ž. Šljivančanin, W. Xu, R. Otero, E. Rauls, I. Stensgaard, E. Lægsgaard, B. Hammer, and F. Besenbacher, Phys. Rev. Lett. **96**, 156104 (2006).

[53] Z. Sun, C. L. Pint, D. C. Marcano, C. Zhang, J. Yao, G. Ruan, Z. Yan, Y. Zhu, R. H. Hauge, and J. M. Tour, Nat. Commun. **2**, 559 (2011).

[54] L. F. Huang, X. H. Zheng, G. R. Zhang, L. L. Li, and Z. Zeng, J. Phys. Chem. C **115**, 21088 (2011).

[55]L. A. Chernozatonskii, P. B. Sorokin, E. É. Belova, J. Brüning, and A. S. Fedorov, JETP Lett. **85**, 77 (2007).
[56]Y. Wang, M. Jaiswal, M. Lin, S. Saha, B. Özyilmaz, and K. P. Loh, ACS Nano **6**, 1018 (2012).
[57]S. Scandolo, M. Bernasconi, G. L. Chiarotti, P. Focher, and E. Tosatti, Phys. Rev. Lett. **74**, 4015 (1995).
[58]F. J. Ribeiro, P. Tangney, S. G. Louie, and M. L. Cohen, Phys. Rev. B **72**, 214109 (2005).
[59]P. L. de Andres, R. Ramírez, and J. A. Vergés, Phys. Rev. B **77**, 045403 (2008).
[60]R. H. Telling, C. P. Ewels, A. A. El-Barbary, and M. I. Heggie, Nat. Mater. **2**, 333 (2003).
[61]A. V. Krasheninnikov and F. Banhart, Nat. Mater. **6**, 723 (2007).
[62]F. Banhart and P. M. Ajayan, Nature (London) **382**, 433 (1996).
[63]M. Zaiser and F. Banhart, Phys. Rev. Lett. **79**, 3680 (1997).
[64]L. Hornekær, E. Rauls, W. Xu, Ž. Šljivančanin, R. Otero, I. Steensgaard, E. Lægsgaard, B. Hammer, and F. Besenbacher, Phys. Rev. Lett. **97**, 186102 (2006).
[65]D. W. Boukhvalov and M. I. Katsnelson, Nano Lett. **8**, 4373 (2008).
[66]A. Krueger, Adv. Mater. **20**, 2445 (2008).